EDGE ARTICLE

Check for updates

Reassessment of N₂ activation by low-valent Ti-amide complexes: a remarkable side-on bridged bis-N₂ adduct is actually an arene adduct†

Daniel N. Huh, [ID] [a] Ross F. Koby, [ID] [a] Zoe E. Stuart, [ID] [a] Rachel J. Dunscomb, [ID] [a] Nathan D. Schley [ID] *[b] and Ian A. Tonks [ID] *[a]

The complex {(TMEDA)₂Li}{[Ti(N(TMS)₂)₂]₂(μ-η²:η²-N₂)₂} (**5-Li**) is the only transition metal N₂ complex ever reported with two side-on N₂ adducts. In this report, the similarity of **5-Li** to a new inverse sandwich toluene adduct {(PhMe)K}{[Ti(N(TMS)₂)₂]₂(μ-PhMe)} (**6-K**) necessitated a re-examination of the structure of **5-Li**. Through a reassessment of the original disordered crystal data of **5-Li** and new independent syntheses brought about through revisitation of the original reaction conditions, **5-Li** has been re-assigned as an inverse sandwich toluene adduct, {(TMEDA)₂Li}{[Ti(N(TMS)₂)₂]₂(μ-PhMe)} (**6-Li**). The original crystal data could be fitted almost equally well to structural solutions as either **5-Li** or **6-Li**, and this study highlights the importance of a holistic examination of modeled data and the need for secondary/complementary analytical methods in paramagnetic inorganic syntheses, especially when presenting unique and unexpected results. In addition, further examination of reduction reactions of Ti[N(TMS)₂]₃ and [(TMS)₂N]₂TiCl(THF) in the presence of KC₈ revealed rich solvent- and counterion-dependent chemistry, including several degrees of N₂ activation (bridging nitride complexes, terminal bridging N₂ complexes) as well as ligand C–H activation.

Introduction

N₂ activation by reduced metal complexes is fundamentally important in understanding how to develop molecular alternatives to the Haber–Bosch process. Myriad N₂ complexes exist across the periodic table, and Ti is no exception:[1] there are examples of end-on and side-on bridging N₂ structures, including fully N–N cleaved nitrides from N₂.[2–7] In some instances, Ti mediated N₂ reduction has also been used to incorporate nitrogen into organic molecules.[8] Recent examples of catalytic N₂ reduction with molecular Ti complexes[2] motivate our renewed interest in further developing the chemistry of low-valent Ti complexes in the context of small molecule activation.

Low-valent Ti complexes can also engender powerful reductive organic transformations,[9–11] such as C(sp³)–H and thiophene oxidative additions,[12,13] arene hydrogenation,[14] and diazene disproportionation.[15] Our group is interested in the synthesis and isolation of various low-valent Ti arene and (hetero)arene adducts, which have been invoked in the catalytic

ᵃDepartment of Chemistry, University of Minnesota – Twin Cities, Minneapolis, MN 55455, USA. E-mail: itonks@umn.edu

ᵇDepartment of Chemistry, Vanderbilt University, Nashville, TN 37235, USA. E-mail: nathan.schley@vanderbilt.edu

synthesis of pyrroles[15–17] *via* nitrene transfer through a formal Ti^II/Ti^IV redox reaction.[18] To date, a variety of Ti^II arene complexes have been isolated (Fig. 1A).[19] For example, Arnold reported a coordinated Ti–toluene complex **1** supported by a *N,N′*-bis(trimethylsilyl)benzamidinate ligand[20] while Ozerov reported a Ti-arene complex **2** supported by a *p-tert*-butyl calix[4]arene ligand.[21] Inverse-sandwich Ti complexes with bridging arenes have also been characterized, as demonstrated by a Cp*Ti adduct **3** reported by Mach[22] and a tripyrrole Ti adduct **4** reported by Gambarotta and Budzelaar.[23] Multidentate intramolecularly bound arene examples have also been reported.[12,24]

Motivated by these examples, we investigated reduction reactions involving a well-known Ti-amido complex, Ti^III[N(TMS)₂]₃,[25] envisioning that the electron-rich, sterically-encumbered (TMS)₂N platform may readily bind free arenes. Herein, we report the synthesis of two inverse sandwich toluene adducts of low-valent Ti {(PhMe)K}{[Ti(N(TMS)₂)₂]₂(μ-PhMe)} (**6-K**) and {(TMEDA)₂Li}{[Ti(N(TMS)₂)₂]₂(μ-PhMe)} (**6-Li**) (Fig. 1B, right). The structures of **6-K** and **6-Li** are surprisingly similar to a previous report of a remarkable example of a doubly side-on bridged N₂ complex, **5-Li** (Fig. 1B, left).[26] **5-Li** was the landmark first report (30 years ago) of a side-on bridged Ti–N₂ complex and has been the only example of a transition metal complex with two side-on bound bridging N₂ ligands reported to date. Structural reassessment of **5-Li** has led us to conclude that this compound was originally mischaracterized as an N₂ adduct and is instead also an inverse sandwich adduct of

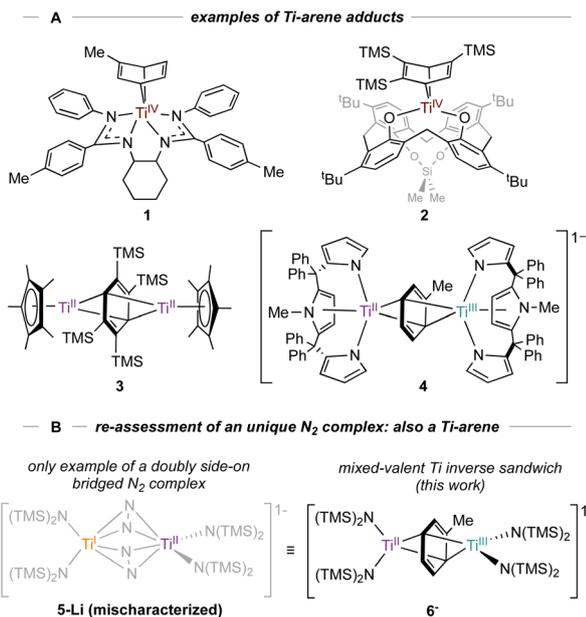© 2022 The Author(s). Published by the Royal Society of Chemistry

Fig. 1   A: Examples of monometallic (1–2) and bimetallic coordinated arenes (3–4). B: New examples of inverse sandwich toluene complexes (6-K and 6-Li) indicate that a reported Ti$_2$–(N$_2$)$_2$ complex 5-Li was originally mischaracterized.[26] Countercations omitted for clarity.

toluene (6-Li). Further exploration of the reduction chemistry of Ti^{III}[N(TMS)$_2$]$_3$ and related low-valent Ti amides under an N$_2$ atmosphere demonstrate a suite of new N$_2$ reduction products, although no side-on N$_2$ adducts.

Results and discussion

Ti^{III}[N(TMS)$_2$]$_3$ was reduced by KC$_8$ in toluene in an effort to isolate a reduced Ti–toluene complex (Fig. 2). When a concentrated toluene solution was passed through a KC$_8$ column,[27] the reaction mixture immediately turned near black yielding the mixed-valent inverse sandwich complex {(PhMe)K} {[Ti(N(TMS)$_2$)$_2$]$_2$(μ-PhMe)} 6-K upon crystallization at −35 °C (40% isolated yield).

The X-ray crystal structure of 6-K is shown in Fig. 2 along with relevant toluene C–C distances and angles. A comparison of 6-K to Ti-arene complexes 1–4 is also shown in Table S15.† In the extreme electronic pictures, 6-K could be described as a Ti^{II}/Ti^{III} complex bridged by a toluene dianion (Fig. 3, left), a Ti^{I}/Ti^{II} complex bridged by a neutral toluene (Fig. 3, right), or a Ti^{III}/Ti^{IV} complex bridged by a toluene tetraanion;[28] any of which could be consistent with the solution-state Evans method magnetic moment of 6-K 1.67μ_B (overall $S = \frac{1}{2}$). The structural metrics indicated that 6-K is best described as a toluene dianion: the C–C bond lengths of 6-K are all remarkably elongated (1.436(4)–1.449(4) Å) and the toluene is significantly folded (dihedral angle = 20.0(2)°), indicating a loss of aromatic character, and ruling out the aromatic neutral or tetraanion toluene ligand descriptions. A picture of the formal oxidation states can also be distinguished by the Ti–N(TMS)$_2$ bond lengths. The Ti^{III}–
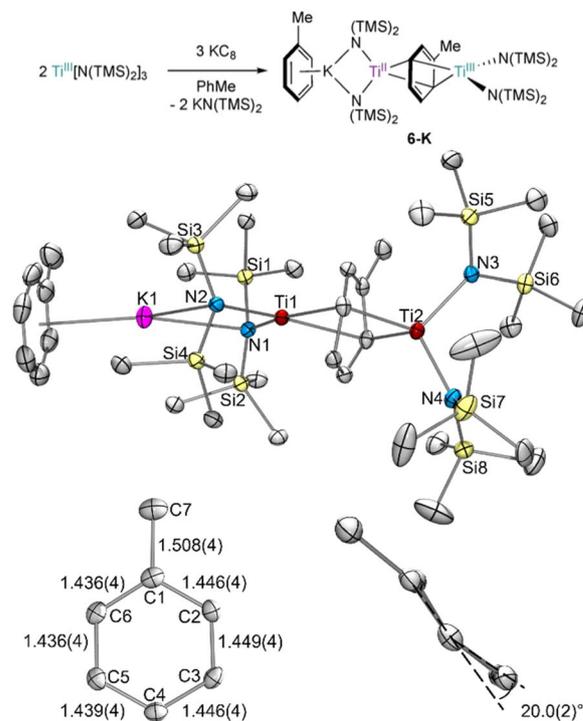

Fig. 2   Top: synthesis of 6-K by KC$_8$ reduction of Ti^{III}[N(TMS)$_2$]$_3$ in toluene. Bottom: crystal structure of 6-K with displacement ellipsoids drawn at the 50% probability level, including zoom-in of the bridging toluene showing the dihedral angle across the C$_5$–C$_6$–C$_1$–C$_2$ and C$_2$–C$_3$–C$_4$–C$_5$ planes. Hydrogen atoms and a disordered TMS group were omitted for clarity. Selected bond distance ranges (Å) and angles (°) are shown in Table S15.†

N(TMS)$_2$ moiety has Ti–N lengths of 2.028(2) and 2.030(2) Å which is consistent with Ti–N(TMS)$_2$ bond lengths in 18 other Ti^{III} compounds (1.929(3) to 2.057(1) Å).[25,26,29–37] The Ti^{II}–N(TMS)$_2$ bearing the (PhMe)K moiety has longer Ti–N(TMS)$_2$ bond lengths which range from 2.129(2) to 2.146(2) Å which is expected for an ion with a lower oxidation state. A similar difference in Ti–N lengths is been found in mixed-valent Ti^{II}/Ti^{III} inverse sandwich 4.[23]

The synthesis of 6-K caused us to re-investigate the very similar formally Ti^{II}/Ti^{III} complex, 5-Li, which was reported to feature a bimetallic Ti–(μ-η^2:η^2-N$_2$)$_2$–Ti core containing two side-on bridging N$_2$ moieties (Fig. 4, left).[26] In the context of 6-K, several features of 5-Li are peculiar. First, the N–N bond lengths in 5-Li (1.379(21) Å) are substantially longer than 37 of 39 reported Ti$_2$–N$_2$ complexes (end-on range: 1.165(5)–1.315(3); side-on range: 1.216(5)–1.226(5)),[1–8,26,33,38–49] although there is one other example of a highly activated end-on Ti$_2$–N$_2$ Tren^{TMS}
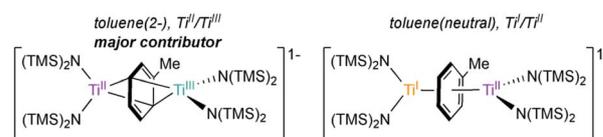

Fig. 3   Electronic representation of 6-K as either Ti^{II}/Ti^{III} bridged by a toluene dianion (left) or Ti^{I}/Ti^{II} bridged by a neutral toluene (right).
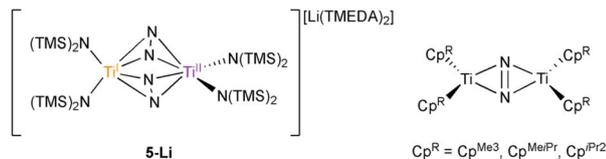
Fig. 4 Reported examples of bimetallic Ti complexes bridged by a side-on N_2 ligand. Left: double side-on Ti–$(N_2)_2$–Ti, **5-Li**, complex.[26] Right: single side-on N_2 titanocene complexes.[5,7]
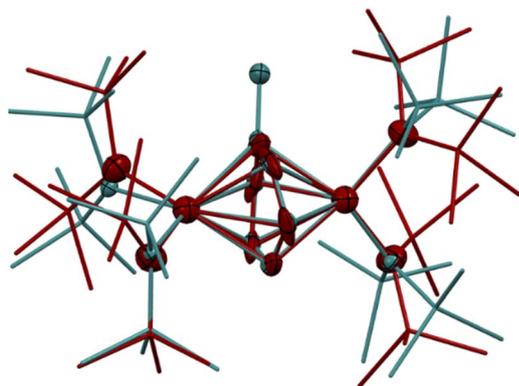

Fig. 5 Overlay of the crystal structures of **5-Li** (maroon) and **6-K** (teal). Displacement ellipsoids are drawn at the 50% probability level. Hydrogen atoms, NTMS$_2$ disorder, and countercations were removed for clarity.

complex with an N–N distance of 1.461(8) Å.[2a] Second, while there are 3 other side-on Ti$_2$–N$_2$ complexes reported (Fig. 4, right),[5,7] **5** is the only reported doubly side-on complex, and in fact the only example of any transition metal containing 2 side-on bridging N_2 ligands. These two N_2 moieties were modelled as disordered over two crystallographically independent nitrogen-atom positions, with a further four positions being generated by symmetry. A close look at the six atomic sites found between the two Ti centers reveals an inverse sandwich motif that is strikingly reminiscent of the structure of **6-K**, and a direct overlay of the Ti coordination spheres of **5-Li** (maroon) and **6-K** (teal) reveal significant overlap (Fig. 5). These features indicate that **5-Li** may have been a mis-assigned arene adduct analogous to **6-K**; in fact, **5-Li** was synthesized in toluene.

Reinspection of the reflection intensities provided as ESI in the original publication led to the discovery of unassigned electron density surrounding the bridging N_2 moieties (Fig. 6) corresponding to a largest difference peak of 0.64 e$^-$ Å^{-3}. Remodeling of the original reflection intensities as a toluene adduct $\{Li(TMEDA)_2\}\{[Ti(NR_2)_2]_2(\mu\text{-PhMe})\}$ (R = TMS) (**6-Li**) across 4 crystallographically-related toluene orientations resulted in slightly improved refinement metrics over the side-on Ti–$(N_2)_2$–Ti moiety **5-Li** (Fig. 7, top). Our model for **6-Li** gives unweighted and weighted R-factors of $R_1 = 0.0601$, w$R_2 = 0.172$, and a largest difference peak of 0.37 e$^-$ Å^{-3} versus $R_1 = 0.0627$, w$R_2 = 0.179$, and 0.64 e$^-$ Å^{-3} for **5-Li**. The relatively modest difference in model quality metrics for such different models ($C_7H_8 = 50$ e$^-$ vs. $2\times N_2 = 28$ e$^-$) is no-doubt influenced by the

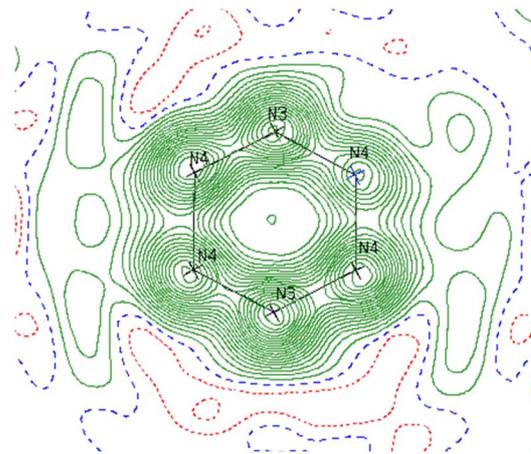**Fig. 6** Contour map of F_{obs} for **5-Li** showing the plane bisecting the Ti–Ti vector. Range: −0.60 to 3.80 e$^-$ Å^{-3} in steps of 0.20. Negative contours are shown in red and positive in green. Residual electron density outside of the N ring indicates likely partial occupancy of another atom at those positions.

relatively poor I/σ, resolution and completeness of the original reflection data, which was not out of the norm for the era in which it was collected.

In order to definitively establish the true identity of **5-Li**, we turned our attention toward resynthesis of **5-Li** in an attempt to collect higher quality X-ray data (Fig. 8). The previous report
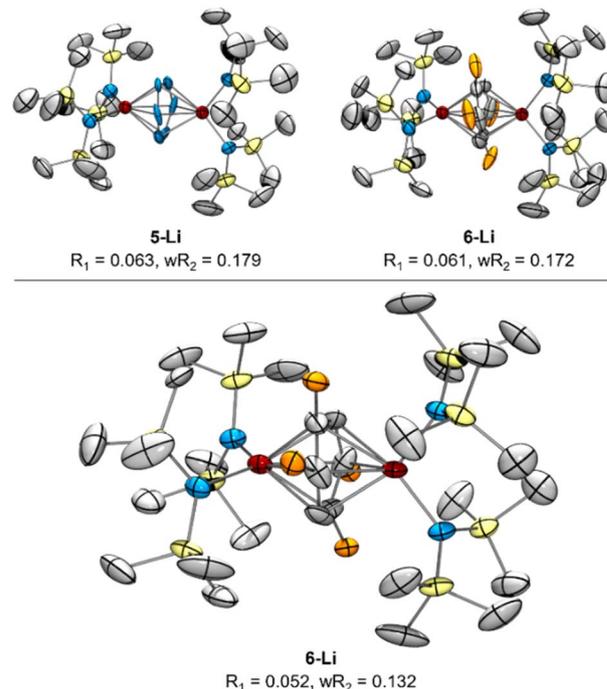

Fig. 7 Top: re-solved SC-XRD of reported **5-Li** reflection data as either **5-Li** (left) or **6-Li** (right) as possible solutions, with displacement ellipsoids drawn at the 50% probability level. Bottom: XRD from new reflection data of re-synthesized **6-Li** following Reaction C from Fig. 8. Orange ellipsoids are disordered Me groups of the toluene dianion in 4 positions. Hydrogen atoms, NTMS$_2$ disorder, and countercations were removed for clarity.
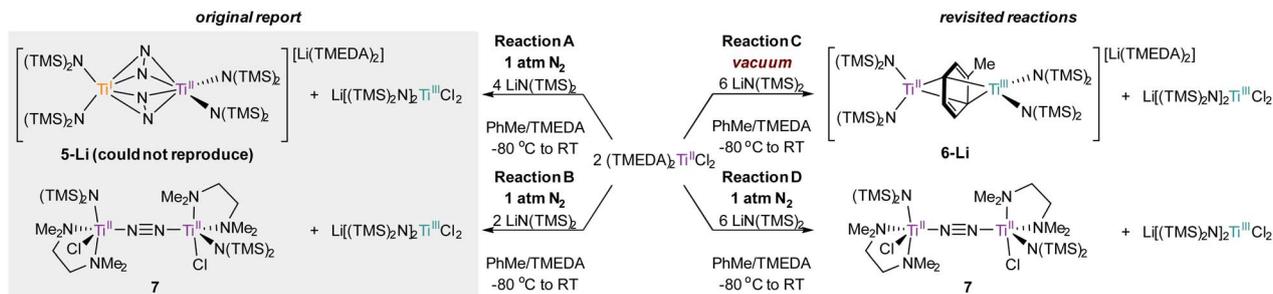
Fig. 8 Previously reported conditions for the synthesis of **5-Li** and **7** (left) and the re-examined reactivity of (TMEDA)$_2$TiCl$_2$ toward N$_2$ and in vacuum conditions for the synthesis of **6-Li** and **7** (right).

described the synthesis of both side-on **5-Li** and an end-on Ti–(μ-η^1:η^1-N$_2$)–Ti complex **7** (Fig. 8, Reactions A and B). Attempts to synthesize **5-Li** under the reported conditions were not successful, with only the end-on bridged **7** produced instead (Fig. 8, Reaction D). In the original synthesis of **5-Li**, there is a discrepancy between the conditions reported in the experimental (under Ar) and in the reaction equation (under N$_2$). When N$_2$ was rigorously excluded by performing the reaction on a Schlenk line under vacuum (Fig. 8, Reaction C) the toluene adduct **6-Li** was isolated. This newly synthesized **6-Li** has an identical unit cell to that reported for **5-Li** with unweighted and weighted R-factors of $R_1 = 0.0519$ and w$R_2 = 0.1320$. Further, the previously published atomic coordinates for **5-Li** can be refined directly against the reflection file obtained for the authentic sample of **6-Li**. Modeling the new XRD data for **6-Li** as **5-Li** gives poorer metrics ($R_1 = 0.0665$ and w$R_2 = 0.1874$). Under this analysis, the largest peak in the difference map is again the unmodeled toluene methyl position which occurs at an identical position in the unit cell, being displaced by only 0.13 Å, a value well below the resolution of the experiment. Finally, hydrolysis of a crystalline sample of the newly-synthesized **6-Li** yielded 57% of toluene by quantitative ^{1}H NMR analysis (ESI, Fig. S2†).

The Raman spectra of **6-K** and **6-Li** are also quite similar (Fig. S26 and S27†), and lack the expected N–N stretch in the 1700 cm^{-1} region that is typical of bridging Ti–N$_2$ complexes (Table S16†).[2a,6,7,50] Further, attempts to calculate (m06 def2svp) optimized structures of [**5**]$^-$ from crystallographic coordinates of **5-Li** result in either a single bridging side-on N$_2$ for a doublet electronic state, or an η^2:η^1 side-on coordinated N$_2$ (ref. 51 and 52) and a terminal end-on N$_2$ for a quartet electronic state (ESI, Pages S26–S34†). The reorganization of the N$_2$ core in these structures provide evidence that a doubly bridging side-on dinitrogen complex like **5** may be unstable for this system. In contrast, geometry optimization of **6-Li** is facile and accurately and precisely models the experimental structure.

Thus, through reassessment of the original data combined with new synthesis and DFT analysis, we can confidently assert that the species previously assigned as the Ti–(μ-η^2:η^2-N$_2$)$_2$–Ti complex **5-Li** is in fact the inverse sandwich complex Ti$_2$–(-PhMe)$^{2-}$ **6-Li**. This result further highlights the importance of looking beyond residual factors when critically analyzing crystallography models, as it is possible to have multiple reasonable

solutions for the same data set. For example, Parkin and co-workers recently determined that the complex [Cd(CO)$_3$(C$_6$H$_3$-Cl)]$_4$ with a reasonable $R_1 = 0.068$ was instead [Re(CO)$_3$(C$_4$N$_2$-H$_3$S)]$_4$ with an $R_1 = 0.034$.[53]

Further reduction reactions with Ti amides

The formation of toluene dianion reaction products **6-Li** and **6-K** provided the incentive to examine the reduction of the pre-formed Ti amide complexes Ti[N(TMS)$_2$]$_3$ (Fig. 9) and [(TMS)$_2$-N]$_2$TiCl(THF) (Fig. 10) under N$_2$ atmosphere.

Preliminary reactivity studies have revealed a suite of N$_2$ activation products, although in many cases the reaction products are inseparable. For example, reduction of Ti[N(TMS)$_2$]$_3$ in hexanes generates a colorless Ti bridging nitride **8**, the product of full N$_2$ cleavage, as an inseparable part of a larger mixture of unidentified products (Fig. 9). Analogous Ti-
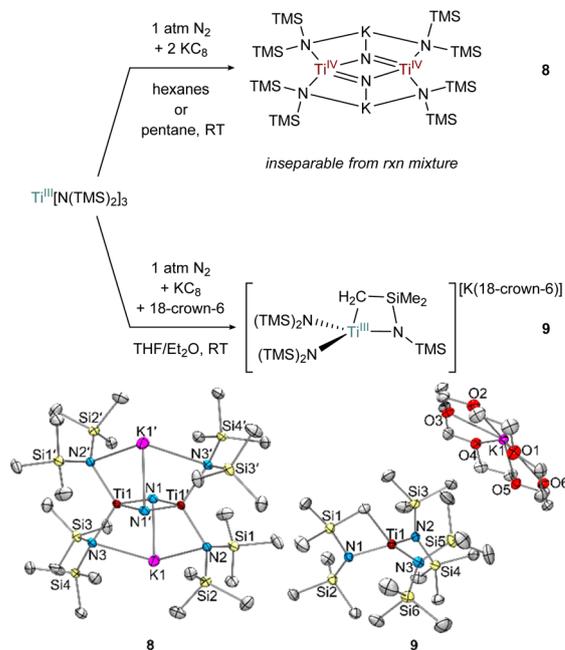

Fig. 9 Top: condition-dependent reduction of Ti[N(TMS)$_2$]$_3$ forming **8** and **9** (top). Bottom: crystal structures of **8** and **9** (bottom) with displacement ellipsoids at the 50% probability level. Hydrogen atoms and were removed for clarity.
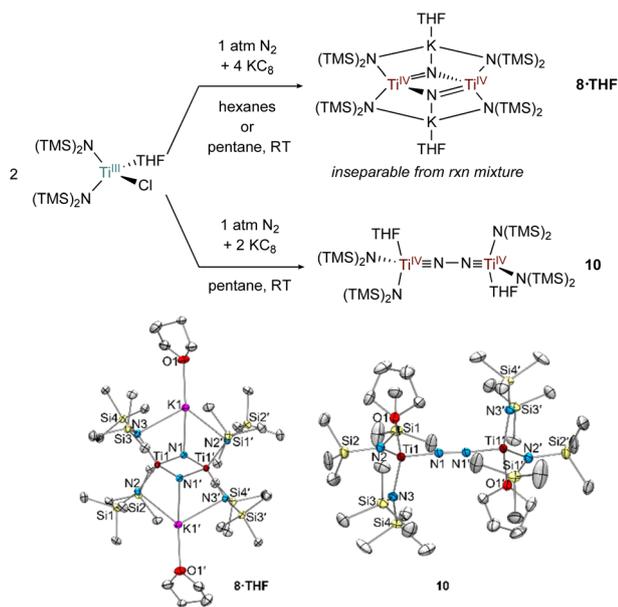
Fig. 10 1 : 2 reduction of [(TMS)$_2$N]$_2$TiCl(THF) using KC$_8$ in the presence of N$_2$ generates **8·THF** and a 1 : 1 reduction in pentane generates **10** (top). Crystal structures of **8·THF** and **10** (bottom) with displacement ellipsoids at the 50% probability level. Hydrogen atoms and disorder were removed for clarity.

Table 1 Selected bond distances (Å) the nitride complexes **8** and **8·THF** and the end-on N$_2$ complexes **7** (ref. 26) and **10**

	Nitride complexes		N$_2$ complexes	
	8	**8·THF**	**7** (ref. 26)	**10**
Ti1–N1	1.825(3)	1.824(1)	1.762(5)	1.763(1)
Ti1–N1′	1.836(3)	1.835(2)		
Ti1–N2	2.073(3)	2.075(1)	2.023(5)	1.995(2)
Ti1–N3	2.092(3)	2.094(1)	—	2.011(1)
N1⋯N1′	2.505(4)	2.503(2)	—	—
N1–N1′	—	—	1.289(9)	1.276(2)

nitride formation has also been reported by Liddle and coworkers using Mg as the reducing agent.[2b] Interestingly, reduction of Ti[N(TMS)$_2$]$_3$ in THF with 18-crown-6 instead generated the Ti^{III} C–H activated product {[(TMS)$_2$N]$_2$Ti[N(TMS)CH$_2$SiMe$_2$]}{K(18-crown-6)}, **9** in 28% isolated yield. Similar examples of cyclometallation from M[N(TMS)$_2$]$_3$ (M = Sc, Ti, Y, Er, Yb, Lu) complexes have been reported.[54–58] In this instance, an equivalent of N(TMS)$_2^-$ likely serves as a base to abstract a proton from the C–H bond, limiting the maximum reaction yield to 50%.

In the attempted reduction reactions with Ti[N(TMS)$_2$]$_3$ the co-product is the highly soluble KN(TMS)$_2$ which led to challenges in cleanly separating the Ti products. To circumvent this issue, reduction reactions of [(TMS)$_2$N]$_2$TiCl(THF) with KC$_8$ were attempted, envisioning that the less soluble KCl co-product would be easier to separate (Fig. 10). Reduction of [N(TMS)$_2$]$_2$TiCl(THF) with 2 equiv. KC$_8$ in hexanes or pentane yielded a THF adduct of a bridging nitride {[(N(TMS)$_2$)$_2$Ti]$_2$(μ-N)$_2$}{K(THF)}$_2$ (**8·THF**), analogous to the reduction of Ti[N(TMS)$_2$]$_3$. Unfortunately, the reaction mixture of **8·THF** was similarly intractable to that of **8**, and identification was only possible by picking single crystals from the mixture. However, reduction of [N(TMS)$_2$]$_2$TiCl(THF) with only 1 equiv. of KC$_8$ in pentane yielded the end-on bridged N$_2$ complex [(N(TMS)$_2$)$_2$-Ti(THF)]$_2$(μ-η^1:η^1-N$_2$) (**10**). Interestingly, further reaction of **10** with excess KC$_8$ did not result in significant formation of **8·THF**.

Selected bond distances from the solid-state structures of **8**, **8·THF**, **7** (ref. 26) and **10** are reported in Table 1. The Ti–N$_{nitride}$ distances in **8** and **8·THF** have nearly identical bond metrical parameters despite containing an additional coordinated THF

to each potassium cation in **8·THF**. The N⋯N distances in **8** and **8·THF** are >2.5 Å, consistent with complete N–N bond scission and the formation of bridging nitrides. Additionally, the Ti–N$_{nitride}$ distances are symmetric, indicating resonance for the Ti≡N double bonds. The N–N bond distances in **10**, (1.276(2) Å), and **7**,[26] (1.289(9) Å), are similar to many other reported Ti–N$_2$–Ti bridging complexes.[2–7] The short Ti–N$_{N_2}$ bond distances in **7** and **10** are (1.76 Å) are indicative of Ti≡N triple bonds, suggesting that a Ti^{IV}≡N–N≡Ti^{IV} electronic structure is predominant in both cases. DFT analysis of **10** further corroborates the Ti≡N triple bond character, as both Ti–N p-bonds can be seen in the HOMO and HOMO − 1 (Fig. S20 and S21†). The Ti–N(TMS)$_2$ distances in **7** and **10** similar to those in the Ti^{IV} nitride compounds **8** and **8·THF**, further indicating Ti^{IV}≡N–N≡Ti^{IV} character in **7** and **10**. These electronic structures are consistent with a recent framework for classifying N$_2$ complexes based on electron counting.[59]

Conclusion

In summary, the bis-N$_2$ side-on complex, **5-Li** is in fact a bridging toluene complex, **6-Li**. This misassignment arises from the modeling of the disorder of the bridging atoms. Despite the reasonable difference in models (C$_7$H$_8$ = 50 e$^-$ vs. 2× N$_2$ = 28 e$^-$) the poor I/σ, resolution and completeness of the original reflection data limited proper interpretation. New experimental and computational analysis of data confirmed the formation of the bridging toluene complex: synthesis under vacuum in toluene yields the same crystals as reported for the incorrectly-assigned N$_2$ adduct, and NMR analysis of the hydrolyzed crystals reveals the presence of toluene. The reassignment of **5-Li** means that there are zero examples of a double-side-on bridging mode of N$_2$ activation, and we posit that this particular bonding motif may not be possible.

Experimental section

General considerations

All syntheses and manipulations described below were conducted under nitrogen with exclusion of air using glovebox, Schlenk-line, and high-vacuum techniques. Ti[N(TMS)$_2$]$_3$,[25] (TMEDA)$_2$TiCl$_2$,[60] and KC$_8$ (ref. 61) were prepared using previously published procedures. TMEDA was vacuum transferred, passed through activated alumina, stored over 4 Å molecular

sieves in the glovebox prior to use. 18-Crown-6 was sublimed prior to use. NMR solvent C_6D_6 was dried over Na^0/Ph_2CO and vacuum transferred before passing through activated alumina in the glovebox. Pentane, hexanes, and toluene were dried on a Pure Process Technology solvent purification system, passed through activated alumina, and stored over activated 4 Å molecular sieves prior to use. ^1H NMR spectra were obtained on a Bruker Avance 400 MHz spectrometer at 298 K. Elemental analysis was shipped to and performed by Midwest Microlab. Attempts to collect elemental analysis on samples of the newly-reported **6-K**, **6-Li**, **9**, and **10** were unsuccessful as these sensitive complexes decomposed during shipment. SC-XRD data of **6-K**, **7**, **8·THF**, **9** and **10** were collected on a Bruker-AXS Venture Photon-III using a Mo source, **6-Li** on a Bruker-AXS Venture Photon-III using a Cu source, and **8** was collected on a Bruker-AXS Smart Apex-II using a Mo source. Crystal and refinement data are available in ESI.† UV-visible absorption spectra were recorded on a HP8453A diode array spectrometer from Unisoku, Scientific Instruments (Osaka, Japan). Raman spectra were obtained at room temperature with excitation at 457 nm (500 mW at source, Cobolt Lasers) through the sample in a J. Young NMR tube using a 135° backscattering arrangement. The collimated Raman scattering was collected using two plano convex lenses (f = 12 cm, placed at an appropriate distance) through appropriate long pass edge filters (Semrock) into an Acton AM-506M3 monochromator equipped with a Princeton Instruments ACTON PyLON LN/CCD-1340 × 400 detector. The detector was cooled to −120 °C prior to the experiments. Spectral calibration was performed using the Raman spectrum of acetonitrile/ toluene 50 : 50 (v/v).[62] Each spectrum was acquired 60 times with 1 s acquisition time, resulting in a total acquisition time of 1 min per spectrum. The collected data was processed using Spectragryph[63] and a multi-point baseline correction was performed for all spectra.

Synthesis of {(PhMe)K}{[Ti(N(TMS)$_2$)$_2$]$_2$(μ-PhMe)} 6-K

In an N_2-filled glovebox, a blue toluene (1.5 mL) solution of Ti[N(TMS)$_2$]$_3$ (196 mg, 0.37 mmol) was passed through a KC_8 filled 7 mm diameter pipette column (5 cm of KC_8) yielding a darkly coloured eluent. An additional 1.5 mL of PhMe was used to wash the KC_8 column. The resulting near black solution was dried *in vacuo* to yield an oil. This oil was extracted with −78 °C pentane (3 × 1.5 mL) and the pentane solution was filtered through glass wool. The resulting pentane solution was then dried *in vacuo* to yield a dark navy-blue powder with colorless crystals (identified as KN(TMS)$_2$ *via* SC-XRD). The powder was then extracted and filtered two additional times with −78 °C pentane (3 × 1.5 mL) until colorless solids were no longer observed. Upon final drying, near black microcrystalline solids of {(PhMe)K}{[Ti(N(TMS)$_2$)$_2$]$_2$(μ-PhMe)} formed (71 mg, 40%). Single crystal X-ray quality crystals were obtained from a concentrated PhMe solution at −35 °C. Evans method: 1.67μ_B.

Synthesis of {(TMEDA)$_2$Li}{[Ti(N(TMS)$_2$)$_2$]$_2$(μ-PhMe)}, 6-Li

In an N_2-filled glovebox, purple (TMEDA)$_2$TiCl$_2$ (300 mg, 0.84 mmol) and colorless LiN(TMS)$_2$ (422 mg, 2.52 mmol) were

added to a Teflon screw cap 100 mL flask. To another 100 mL Teflon screw cap flask, toluene (10 mL) and TMEDA (0.5 mL) were added. Both flasks were sealed, removed from the glove-box, and placed on a high-vac line. The flask containing the solid (TMEDA)$_2$TiCl$_2$ and LiN(TMS)$_2$ were placed under vacuum (10^{-4} torr) for 3 h. The PhMe/TMEDA solution was degassed *via* three 1 h freeze–pump–thaw cycles. The PhMe/TMEDA solution was vacuum transferred to the flask containing solids using a −78 °C bath. The flask was then sealed and the purple mixture was stirred and warmed to room temperature. After 30 min of stirring, the purple mixture turned brown. After 1 d, degassed Et$_2$O (*via* three 1 h, freeze–pump–thaw cycles) was vacuum transferred to the frozen brown mixture. Upon thawing, an Et$_2$O layer on the brown solution formed. The sealed flask was stored in a −30 °C freezer. After 1 d, both colorless and brown crystals formed. The colorless crystals were identified as [Li(TMEDA)$_2$] {[(TMS)$_2$N]$_2$TiCl$_2$} *via* unit-cell analysis (CSD Refcode: JOHBAJ). A full dataset of the brown crystals were collected and identified as {(TMEDA)$_2$Li}{[Ti(N(TMS)$_2$)$_2$]$_2$(μ-PhMe)}, **6-Li**.

Synthesis of [(TMEDA)Ti(N(TMS)$_2$)Cl]$_2$(μ-N$_2$), 7

In an N_2-filled glovebox, purple (TMEDA)$_2$TiCl$_2$ (300 mg, 0.84 mmol) and colorless LiN(TMS)$_2$ (421 mg, 2.52 mmol) were added to a 100 mL flask and chilled to −78 °C. To this flask, −78 °C toluene (10 mL) and TMEDA (0.5 mL) were added. The purple mixture was stirred and warmed to room temperature. The purple mixture turned brown within minutes. After 1 d, the brown solution was layered with Et$_2$O and placed in a −30 °C freezer. After 1 d, colorless and brown crystals formed. The colorless crystals were identified as [Li(TMEDA)$_2$]{[(TMS)$_2$N]$_2$-TiCl$_2$} *via* unit-cell analysis (CSD Refcode: JOHBAJ). A full dataset of the brown crystals were collected and identified as [(TMEDA)Ti(N(TMS)$_2$)Cl]$_2$(μ-N$_2$), **7**.

Synthesis of reaction mixture containing 8

In an N_2-filled glovebox, a blue Ti[N(TMS)$_2$]$_3$ (100 mg, 0.19 mmol) solution in hexanes (5 mL) was added to KC_8 (54 mg, 0.38 mmol) forming a darkly coloured mixture. After stirring for 3 d, the near black mixture was filtered through Celite to remove graphite. The resulting near black solution was placed in a −30 °C freezer. After 1 d, colourless crystals covered in tar formed from the near black solution and were identified as the bridging nitride complex **8**. Crystals of K[N(TMS)$_2$] were also identified in the mixture by matching the unit-cell (CSD Refcode: VETFOP).

Synthesis of reaction mixture containing 8·THF

In an N_2-filled glovebox, a light blue [(TMS)$_2$N]$_2$TiCl(THF) (100 mg, 0.21 mmol) solution in hexanes (5 mL) was added to KC_8 (57 mg, 0.42 mmol) forming a darkly coloured mixture. After stirring for 3 d, the black mixture was filtered through Celite to remove graphite. The resulting solution was placed in a −30 °C freezer. After 1 d, colorless crystals covered in tar formed from the near black solution and were identified as the bridging nitride complex **8·THF**.

Synthesis of [K(18-crown-6)]{[(TMS)$_2$N]$_2$Ti[N(TMS)(SiMe$_2$CH$_2$)]}, 9

In an N$_2$-filled glovebox, a blue 3 : 1 Et$_2$O : THF (4 mL) solution of Ti[N(TMS)$_2$]$_3$ (100 mg, 0.19 mmol) was added dropwise to a dark blue 3 : 1 Et$_2$O : THF (10 mL) mixture of 18-crown-6 (52 mg, 0.19 mmol) and KC$_8$ (27 mg, 0.19 mmol) forming a darkly coloured mixture. After 4 d of stirring, the dark green mixture was filtered though Celite to remove graphite and the dark green solution was placed under vacuum. The resulting green oil was redissolved in Et$_2$O (1 mL) and layered into pentane (10 mL) and placed in a −30 °C freezer. After 1 d, green single-crystals formed and were identified as [K(18-crown-6)]{[(TMS)$_2$N]$_2$Ti[N(TMS)(SiMe$_2$CH$_2$)]}, 9, *via* SC-XRD (44 mg, 28%).

Modified synthesis of [(TMS)$_2$N]$_2$TiCl(THF)[36]

In an N$_2$-filled glovebox, TiCl$_3$(THF)$_3$ (1006 mg, 2.7 mmol) and LiN(TMS)$_2$ (918 mg, 5.4 mmol) were stirred in pentane (50 mL) for 1 h. The resulting light blue mixture was filtered through Celite twice to remove LiCl. The clear blue solution was placed in a −30 °C freezer. After 1 d, light blue crystals formed in a dark green solution. The green solution as decanted away and the light blue crystals were washed with −78 °C pentane (3 × 2 mL) and isolated (983 mg, 76%).

Synthesis of [(TMS)$_2$N$_2$Ti(THF)]$_2$(μ-N$_2$), 10

In an N$_2$-filled glovebox, light blue pentane (5 mL) solution of [(TMS)$_2$N]$_2$TiCl(THF) (200 mg, 0.42 mmol) was added to KC$_8$ (57 mg, 0.42 mmol) forming a darkly coloured mixture. After stirring for 1 d, the mixture was filtered through Celite to remove graphite and KCl. The resulting brown solution was concentrated to ∼0.5 mL of pentane and placed in a −30 °C freezer. After 1 d, brown single-crystals formed and were identified as [(TMS)$_2$N$_2$Ti(THF)]$_2$(μ-N$_2$), 10. The crystals were washed with −78 °C pentane and isolated (34 mg, 18%). Crystalline yields are low due to the high solubility of this compound. ^{1}H (400 MHz, C$_6$D$_6$, 25 °C, δ, ppm) 4.17 (s, 8H, THF) 1.46 (m, 8H, THF), 0.43 (s, 72H, SiMe$_3$).

Data availability

All experimental and computational data is available as a part of the ESI.†

Author contributions

Daniel N. Huh: conceptualization, investigation, formal analysis, writing – original draft, writing – review & editing, funding acquisition. Ross F. Koby: investigation, formal analysis, writing – original draft, writing – review & editing. Zoe E. Stuart: investigation. Rachel J. Dunscomb: investigation. Nathan D. Schley: investigation, formal analysis, writing – original draft, writing – review & editing. Ian A. Tonks: conceptualization, writing – review & editing, supervision, funding acquisition.

Conflicts of interest

There are no conflicts to declare.

Acknowledgements

References

1 D. Singh, W. R. Buratto, J. F. Torres and L. J. Murray, *Chem. Rev.*, 2020, **120**, 5517–5581.

2 (a) L. R. Doyle, A. J. Wooles, L. C. Jenkins, F. Tuna, E. J. L. McInnes and S. T. Liddle, *Angew. Chem., Int. Ed.*, 2018, **57**, 6314–6318; (b) L. R. Doyle, A. J. Wooles and S. T. Liddle, *Angew. Chem., Int. Ed.*, 2019, **58**, 6674–6677.

3 T. E. Hanna, E. Lobkovsky and P. J. Chirik, *J. Am. Chem. Soc.*, 2004, **126**, 14688–14689.

4 T. E. Hanna, E. Lobkovsky and P. J. Chirik, *J. Am. Chem. Soc.*, 2006, **128**, 6018–6019.

5 T. E. Hanna, W. H. Bernskoetter, M. W. Bouwkamp, E. Lobkovsky and P. J. Chirik, *Organometallics*, 2007, **26**, 2431–2438.

6 T. E. Hanna, E. Lobkovsky and P. J. Chirik, *Organometallics*, 2009, **28**, 4079–4088.

7 S. P. Semproni, C. Milsmann and P. J. Chirik, *Organometallics*, 2012, **31**, 3672–3682.

8 Y. Nakanishi, Y. Ishida and H. Kawaguchi, *Angew. Chem., Int. Ed.*, 2017, **56**, 9193–9197.

9 S. Fortier and A. Gomez-Torres, *Chem. Commun.*, 2021, **57**, 10292–10316.

10 A. Gomez-Torres, C. Saucedo and S. Fortier, *Arene Complexes of Group 4 Metals. Comprehensive Organometallic Chemistry IV*, ed. K. Meyer, D. O'Hare and G. Parkin, Elsevier Ltd, 2022, pp. 502–549.

11 G. B. Wijeratne, E. M. Zolnhofer, S. Fortier, L. N. Grant, P. J. Carroll, C.-H. Chen, K. Meyer, J. Krzystek, A. Ozarowski, T. A. Jackson, D. J. Mindiola and J. Telser, *Inorg. Chem.*, 2015, **54**, 10380–10397.

12 J. R. Aguilar-Calderón, A. J. Metta-Magaña, B. Noll and S. Fortier, *Angew. Chem., Int. Ed.*, 2016, **55**, 14101–14105.

13 A. Gómez-Torres, J. R. Aguilar-Calderón, C. Saucedo, A. Jordan, A. Metta-Magaña, B. Pinter and S. Fortier, *Chem. Commun.*, 2020, **56**, 1545–1548.

14 A. Gómez-Torres, J. R. Aguilar-Calderón, A. M. Encerrado-Manriquez, M. Pink, A. J. Metta-Magaña, W.-Y. Lee and S. Fortier, *Chem.–Eur. J.*, 2020, **26**, 2803–2807.

15 Z. W. Gilbert, R. J. Hue and I. A. Tonks, *Nat. Chem.*, 2016, **8**, 63–68.

16 Z. W. Davis-Gilbert, X. Wen, J. D. Goodpaster and I. A. Tonks, *J. Am. Chem. Soc.*, 2018, **140**, 7267–7281.

17 J. Guo, X. Deng, C. Song, Y. Lu, S. Qu, Y. Dang and Z.-X. Wang, *Chem. Sci.*, 2017, **8**, 2413–2425.

18 I. A. Tonks, *Acc. Chem. Res.*, 2021, **54**, 3476–3490.

19 S. Fortier, A. Gomez-Torres and C. Saucedo, in *Reference Module in Chemistry, Molecular Sciences and Chemical Engineering*, Elsevier, 2021, DOI: 10.1016/B978-0-12-820206-7.00012-3.

20 J. R. Hagadorn and J. Arnold, *Angew. Chem., Int. Ed.*, 1998, **37**, 1729–1731.

21 O. V. Ozerov, B. O. Patrick and F. T. Ladipo, *J. Am. Chem. Soc.*, 2000, **122**, 6423–6431.

22 R. Gyepes, J. Pinkas, I. Císařová, J. Kubišta, M. Horáček and K. Mach, *RSC Adv.*, 2016, **6**, 94149–94159.

23 G. B. Nikiforov, P. Crewdson, S. Gambarotta, I. Korobkov and P. H. M. Budzelaar, *Organometallics*, 2007, **26**, 48–55.

24 J. N. Boynton, J.-D. Guo, F. Grandjean, J. C. Fettinger, S. Nagase, G. J. Long and P. P. Power, *Inorg. Chem.*, 2013, **52**, 14216–14223.

25 M. A. Putzer, J. Magull, H. Goesmann, B. Neumüller and K. Dehnicke, *Chem. Ber.*, 1996, **129**, 1401–1405.

26 R. Duchateau, S. Gambarotta, N. Beydoun and C. Bensimon, *J. Am. Chem. Soc.*, 1991, **113**, 8986–8988.

27 W. J. Evans, *Organometallics*, 2016, **35**, 3088–3100.

28 D. Patel, F. Tuna, E. J. L. McInnes, J. McMaster, W. Lewis, A. J. Blake and S. T. Liddle, *Dalton Trans.*, 2013, **42**, 5224–5227.

29 C. R. Stennett, J. C. Fettinger and P. P. Power, *Inorg. Chem.*, 2020, **59**, 1871–1882.

30 C. R. Stennett and P. P. Power, *Inorg. Chem.*, 2021, **60**, 18503–18511.

31 M. A. Putzer, R. J. Lachicotte and G. C. Bazan, *Inorg. Chem. Commun.*, 1999, **2**, 319–322.

32 J. J. H. Edema, R. Duchateau, S. Gambarotta, R. Hynes and E. Gabe, *Inorg. Chem.*, 1991, **30**, 154–156.

33 N. Beydoun, R. Duchateau and S. Gambarotta, *J. Chem. Soc., Chem. Commun.*, 1992, 244–246, DOI: 10.1039/C39920000244.

34 B. C. Bailey, F. Basuli, J. C. Huffman and D. J. Mindiola, *Organometallics*, 2006, **25**, 2725–2728.

35 C. C. Quadri, K. W. Tornroos and E. Le Roux, *IUCrData*, 2017, **2**, x171488.

36 L. Scoles and S. Gambarotta, *Inorg. Chim. Acta*, 1995, **235**, 375–380.

37 R. K. Minhas, L. Scoles, S. Wong and S. Gambarotta, *Organometallics*, 1996, **15**, 1113–1121.

38 R. D. Sanner, D. M. Duggan, T. C. McKenzie, R. E. Marsh and J. E. Bercaw, *J. Am. Chem. Soc.*, 1976, **98**, 8358–8365.

39 J. M. de Wolf, R. Blaauw, A. Meetsma, J. H. Teuben, R. Gyepes, V. Varga, K. Mach, N. Veldman and A. L. Spek, *Organometallics*, 1996, **15**, 4977–4983.

40 A. Scherer, K. Kollak, A. Lützen, M. Friedemann, D. Haase, W. Saak and R. Beckhaus, *Eur. J. Inorg. Chem.*, 2005, **2005**, 1003–1010.

41 P. P. Fontaine, B. L. Yonke, P. Y. Zavalij and L. R. Sita, *J. Am. Chem. Soc.*, 2010, **132**, 12273–12285.

42 J. R. Hagadorn and J. Arnold, *J. Am. Chem. Soc.*, 1996, **118**, 893–894.

43 S. M. Mullins, A. P. Duncan, R. G. Bergman and J. Arnold, *Inorg. Chem.*, 2001, **40**, 6952–6963.

44 G. Bai, P. Wei and D. W. Stephan, *Organometallics*, 2006, **25**, 2649–2655.

45 Y. Sekiguchi, F. Meng, H. Tanaka, A. Eizawa, K. Arashiba, K. Nakajima, K. Yoshizawa and Y. Nishibayashi, *Dalton Trans.*, 2018, **47**, 11322–11326.

46 B. Wang, G. Luo, M. Nishiura, S. Hu, T. Shima, Y. Luo and Z. Hou, *J. Am. Chem. Soc.*, 2017, **139**, 1818–1821.

47 W. A. Chomitz and J. Arnold, *Chem. Commun.*, 2007, 4797–4799, DOI: 10.1039/B709763H.

48 R. Baumann, R. Stumpf, W. M. Davis, L.-C. Liang and R. R. Schrock, *J. Am. Chem. Soc.*, 1999, **121**, 7822–7836.

49 T. Kurogi, Y. Ishida and H. Kawaguchi, *Chem. Commun.*, 2013, **49**, 11755–11757.

50 F. Studt, N. Lehnert, B. E. Wiesler, A. Scherer, R. Beckhaus and F. Tuczek, *Eur. J. Inorg. Chem.*, 2006, 291–297.

51 M. D. Fryzuk, S. A. Johnson and S. J. Rettig, *J. Am. Chem. Soc.*, 1998, **120**, 11024–11025.

52 D. Pun, E. Lobkovsky and P. J. Chirik, *J. Am. Chem. Soc.*, 2008, **130**, 6047–6054.

53 E. Amemiya, A. Loo, D. G. Shlian and G. Parkin, *Chem. Sci.*, 2020, **11**, 11763–11776.

54 M. Karl, K. Harms, G. Seybert, W. Massa, S. Fau, G. Frenking and K. Dehnicke, *Z. Anorg. Allg. Chem.*, 1999, **625**, 2055–2063.

55 M. A. Putzer, B. Neumüller and K. Dehnicke, *Z. Anorg. Allg. Chem.*, 1998, **624**, 1087–1088.

56 F. Han, J. Zhang, W. Yi, Z. Zhang, J. Yu, L. Weng and X. Zhou, *Inorg. Chem.*, 2010, **49**, 2793–2798.

57 M. Niemeyer, *Inorg. Chem.*, 2006, **45**, 9085–9095.

58 M. Fang, J. E. Bates, S. E. Lorenz, D. S. Lee, D. B. Rego, J. W. Ziller, F. Furche and W. J. Evans, *Inorg. Chem.*, 2011, **50**, 1459–1469.

59 L. S. Yamout, M. Ataya, F. Hasanayn, P. L. Holland, A. J. M. Miller and A. S. Goldman, *J. Am. Chem. Soc.*, 2021, **143**, 9744–9757.

60 E. M. Zolnhofer, G. B. Wijeratne, T. A. Jackson, S. Fortier, F. W. Heinemann, K. Meyer, J. Krzystek, A. Ozarowski, D. J. Mindiola and J. Telser, *Inorg. Chem.*, 2020, **59**, 6187–6201.

61 D. E. Bergbreiter and J. M. Killough, *J. Am. Chem. Soc.*, 1978, **100**, 2126–2134.

62 *Standard Guide for Raman Shift Standards for Spectrometer Calibration, ASTM E1840-96(2007)*, ASTM International, West Conshohocken, PA, 2007.

63 F. Menges, *Spectragryph – optical spectroscopy software, version 1.2.15*, 2021, http://www.effemm2.de/spectragryph/.